Hindawi
International Journal of Aerospace Engineering
Volume 2022, Article ID 2171471, 14 pages
https://doi.org/10.1155/2022/2171471

Research Article

Dynamic Characteristics of LOX/Kerosene Variable Thrust Liquid Rocket Engine Test System Based on General Modular Simulation Method

Qingdong Su,[1,2] **Jinjin Wang**,[1] **Mingxia Yan**,[1,2] **Zhensheng Sun**,[1] **Weifeng Huang**,[2] **and Bailin Zha**[3]

[1]*Missile Engineering College, Rocket Force University of Engineering, Xi'an 710025, China*
[2]*Department of Mechanical Engineering, Tsinghua University, Beijing 100084, China*
[3]*Project Management Center, Beijing 100085, China*

Correspondence should be addressed to Jinjin Wang; hdwangjinjin@163.com and Bailin Zha; zhabailin@163.com

Received 21 August 2022; Revised 16 November 2022; Accepted 29 November 2022; Published 15 December 2022

Academic Editor: Jinyang Xu

For the research demand of reusable LOX/kerosene variable thrust liquid rocket engine, a test system with electric displacement pumps is designed and a multidisciplinary modular dynamic simulation method based on AMESim platform is used to analyze the system. The method comprehensively considers the characteristics of complex components in the engine and realizes the fast module assembly and variable step size solution. Considering the combustion model of thrust chamber, the positive displacement pump model with complex leakage channels, and the cooling jacket heat transfer model, the component dynamic equations are deduced and the final model simulation results reveal that the system has a smooth ignition, stage turning, and shutdown process. The thrust can reach 6900 N in high working condition and the variable thrust ratio is 5 : 1. The dynamic characteristics of the system show that the performance error of main pump components is less than 5%, the maximum average temperature rise of the thrust chamber coolant is about 28°C, and the time of stage adjustment is within 300 ms, which mean the overall design of the system is reasonable. Although the accumulation of LOX before kerosene injection can adversely affect the temperature of the thrust chamber, large pressure pulses do not occur due to the ignitor's duty flame. Moreover, the pintle injectors based on PID control can effectively stabilize the pressure drop at lower conditions. The system and the simulation method provide important support for the actual engine test and the general LRE dynamic characteristics analysis.

1. Introduction

The liquid rocket engine (LRE) is the main power for rockets and missiles. With the opening of space exploration policies, the demand for the development of reusable LRE is increasing in recent years [1, 2]. Among them, the liquid oxygen (LOX)/kerosene rocket engine has been widely studied and applied in China and Russia for a long time, mainly due to their outstanding advantages in density specific impulse [3]. Recently, the LOX/kerosene rocket engine ("Merlin") deployed on reusable "Falcon" rockets developed by the SpaceX company in America has shown perfect performance and received unprecedented attention [4].

At present, a test system of the LRE provides the similar working state in the actual flight process and gives the direct support for parameters confirmation and technical verification of the thrust chamber and other components [5]. However, the actual test is still time-consuming, costly, and dangerous, so the combination of simulation and test is an important research method for the new LRE [6]. In the preresearch stage, the dynamic characteristic simulation can be used to design the system structure and evaluate the time sequence. In the verification stage, the simulation is an

important method for parameter adjustment, time sequence optimization, and fault analysis. In the equipment stage, it can also be used for health monitoring and linear or nonlinear intelligent control research [7, 8].

In the early stages of research on LRE and its test system characteristics, some basic ordinary differential equations make up the special programs. Typical examples are the start-up process model of the Agena rocket engine in US Air Force Rocket Propulsion Laboratory [9], the neural network program for the Space Shuttle Main Engine (SSME) start-up characteristics in Lewis Research Center [10], dynamic characteristic simulation program for LE-5 and LE-7 engines, [11] and so on. Besides, Zhang et al. compiled the static/dynamic model of the YF-20 LRE based on MATLAB, and a BP neural network was used to analyze the failure [12]. But these special programs rely on clear data formats and transfer relationships, which can be briefly summarized as "one machine, one program." These nongeneric simulation methods cannot meet the requirements of rapid tasks on complex system simulation.

With the development of software engineering technology, general simulation programs have become the main research direction. Li et al. reviewed the technological progress of the dynamic characteristics simulation, and the result can be summarized as "graphical interface, independent simulation environment, metamodel abstraction, and high reusability" [13]. Some representative achievements are German DRL company modular engine analysis system [14], ROCETS in NASA Marshall Space Flight Center and its improved software ESAY5x [15], CARINS in French [16], and Japan LE-7A Engine MPI parallel software REDS [17]. In terms of commercial platforms, there are EcosimPro of Spain's EAI Company, the aerospace propulsion system simulation module ESPSS [18] jointly developed by the European Space Agency, AMESim of Siemens company [19], and so on. China's National University of Defense Technology [20], Beihang University [21], and Xi'an Aerospace Propulsion Institute [22] have developed a variety of general simulation software based on the C language or Simulink tools. Recently, a software based on the Modelica language Mworks [23] has been used in some LRE programs, which significantly improved the engineering efficiency. However, except for AMESim, most of those platforms are in the initial stage of small-scale application.

As a powerful system simulation software, AMESim has the SSME and RL-10A models in its liquid propulsion library. Based on the AMESim platform, Li [24] and Zheng et al. [25] did some research on the dynamic characteristics of an expansion cycle LOX/methane engine. Zhang et al. [26] conducted a research on the cryogenic wind tunnel, in which dynamic characteristics of the liquid nitrogen supply system were analyzed. Liu et al. [27] and Cui et al. [28] conducted the systematic modeling of the electric pump LOX/kerosene engine, which further confirmed the reliability of the method.

Aiming at the requirements of the ground test of the reusable variable thrust LRE, an LOX/kerosene engine test system with electric positive displacement pumps is designed. Based on the modular modeling and simulation method, the dynamic characteristic model of the test system is established on the AMESim platform. The input parameters are derived from the actual engineering parameters and the test results in cold condition. The two-phase characteristics of the cryogenic LOX pipelines and the fine structure of pumps are considered in the model, and the heat transfer characteristics of the thrust chamber are calculated. Then, the dynamic performance of the system under pretest condition and variable thrust conditions is analyzed, and finally, the guiding conclusion for further implementation of ignition test is given.

2. Engine Test System

2.1. Working Medium Supply System. The structure of the test system is shown in Figure 1, and the main parameters are listed in Table 1. The medium supply system consists of 6 subsystems, which provide the LRE with a variety of working fluids such as LOX, kerosene, coolant, control gas, oxygen, and hydrogen for ignition torch. The water is used as the cooling medium, and the repeated ignition relies on an electronic ignition torch.

Kerosene subsystem: kerosene is pressurized by the piston pump and fed into the injection unit through the main valve and one-way valve from the tank. The flow is controlled by adjusting the frequency converter of the pump.

LOX subsystem: the subsystem consists of an adiabatic tank, a pump, a mass flowmeter, and some pipelines. LOX is pressurized by a three-row piston pump, and the flow is regulated by the pump frequency conversion.

Hydrogen subsystem: the subsystem provides fuel for the ignition torch and includes a hydrogen cylinder group, a globe valve, a pressure reducing valve, a sonic nozzle, and a flashback preventer. The flow is controlled by an automatic pressure-reducing valve and a sonic nozzle.

Oxygen subsystem: the subsystem provides oxidant for the ignition torch, and its structure is similar to the hydrogen subsystem.

Nitrogen subsystem: the subsystem can provide control gas and purge gas.

Coolant subsystem: the subsystem provides coolant for the thrust chamber and helps to cool down the exhaust emission system and reduce the noise. The flow is controlled by adjusting the rotational speed of the centrifugal pump.

2.2. Thrust Chamber. The thrust chamber is the main test objective. According to the task document, the theoretical condition in the first pretest is offset from optimal mixing ratio. The pretest condition refers to the test condition with low mixing ratio and total flow, which means that the temperature and pressure of the combustion chamber are low under this condition. The pretest indicators are as follows: the thrust is about 4000~4500 N, the chamber pressure is 3 MPa, and the temperature is 2000 K.

Based on the fixed pressure, the theoretical temperature, specific impulse, products, and other parameters under different mixing ratios can be obtained by chemical equilibrium calculation (CEA). The thermodynamic results are shown in Table 2 with a mixing ratio of 1.3.

The relationship among flow $\dot{m}$, throat area A_t, and combustion chamber pressure P_c are derived from the specific impulse I_{sp} and characteristic velocity C^*.

$$\dot{m} = \frac{F}{I_{sp}},$$
$$A_t = \frac{\dot{m}C^*}{P_c}. \tag{1}$$

The total flow in the pretest condition is 2.03 kg/s, and the diameter of the throat is 36.24 mm. Then, the flow of LOX and kerosene can be determined by the mixing ratio. Considering implementation issues, the diameter of the throat is set to 36 mm and the expansion ratio is 5.

The geometric parameters such as the volume and diameter of the combustion chamber are related to the characteristic length ($L^* = 2\text{m}$) and relative flow density ($r_s^- = 1.8 \times 10^{-3} P_c$).

$$V_c = L^* A_t,$$
$$D_c = \sqrt{\frac{4A_c}{\pi}} = \sqrt{\frac{4}{\pi}\frac{\dot{m}}{r_s}}. \tag{2}$$

The minimum volume V_c is 2.036 L, and the minimum diameter D_c is 68.7 mm. The final parameters of the thrust chamber constrained by the lower limit of the total volume are shown in Table 3.

As shown in Figure 2, the profile of the thrust chamber can be divided into a circle contraction section and a bell-shaped nozzle. Considering the test requirements on ground and high altitude, the nozzle is divided into two sections according to the expansion ratio of 5 ($D_1 = 80\text{mm}$) and 50 ($D_2 = 254\text{mm}$). The front section has a milled groove regenerative cooling structure made of copper (CuCr1Zr), and the tail section is a nozzle cooled by radiation.

The gas residence time is as follows:

$$\tau_s = \frac{m_c}{\dot{m}} = \frac{p_c V_c}{R_c T_c \dot{m}} = \frac{p_c V_c M_c}{\mathrm{R}_0 T_c \dot{m}}. \tag{3}$$

In the equation, R_0 is the general gas constant, and the average molar mass of the gas M_c is 16.275 kg/mol. So, the gas residence time is about 6.27 ms, which conforms to the design requirement (1~8 ms).

The head of the thrust chamber has a structure with 8 coaxial centrifugal injectors. As shown in Figure 3, the high-pressure kerosene is sprayed through the outer annular seam, and the ignition torch is assembled in the center.

In order to get more deep adjustment of the thrust, the injector is further modified to a stepper motor-driven pintle injector. The actuating mechanism automatically adjusts the oxidant and fuel injection based on the feedback parameters (injection pressure drop ratio), which are output by the PID controller. These measures can keep the chamber in good atomization and combustion state.

2.3. Measurement and Control Methods. The main measured parameters are the pressure, flow, and temperature of some nodes shown in Figure 1. The thrust test bench, as the main component for measurement, consists of slide rails, fixtures, and strain-type thrust sensors. The engine is horizontally arranged, and sensors and control valves are located at the front of the bench.

Figure 4 shows the main sequence of start-up and shutdown of the system, which is verified by the adjustment test in cold state.

The ignition torch works first to establish the on-duty flame, and the time difference between the backflow of the propellant circuit, the emptying valve, and the main valve is set to be 50 ms to prevent the system from overpressure.

3. Numerical Model

The former Soviet Union/Russian scholars conducted an in-depth research on engine mathematical theory [29]. They deduced the basic dynamic equations of the LRE, verifying that it is important to apply system simulations before the actual ignition test. Based on the IRC method [30], some detailed dynamic models such as pipelines, thermal components, pumps, valves, and throttling elements of the engine test system are established. The ignition torch and gas blowing components are simplified in the simulation.

3.1. Pipeline Numerical Model. According to the target for low-frequency analysis of the system, the main pipelines of LOX, kerosene, and coolant are set as C, IR, or R elements [30]. These elements consider the capacitive, inertial, and resistive properties, respectively.

The equations of pressure and temperature considering the heat exchange are

$$\frac{\mathrm{dp}}{\mathrm{dt}} = \beta_{\mathrm{eff}}\left[\frac{1}{\rho}\frac{d\rho}{\mathrm{dt}} + \alpha\frac{\mathrm{dT}}{\mathrm{dt}}\right],$$
$$\frac{\mathrm{dT}}{\mathrm{dt}} = \frac{\mathrm{dhin} + \sum \mathrm{dmh}_i - h\sum \mathrm{dm}_i}{c_p \cdot \rho \cdot V_{\mathrm{eff}}} + \frac{\alpha \cdot T}{c_p \cdot \rho}\frac{\mathrm{dp}}{\mathrm{dt}}, \tag{4}$$

where ρ is the density, $\sum \mathrm{dm}_i$ is the total input mass flow, $\sum \mathrm{dmh}_i$ is the input total enthalpy, β_{eff} is the combined bulk modulus, V_{eff} is the effective volume, and dhin is the heat exchange between the pipeline and the outside.

Considering the elasticity of fluid and pipeline wall, the combined bulk modulus is

$$\beta_{\mathrm{eff}} = \left(\frac{1}{\beta_{\mathrm{fluid}}} + \frac{w_{\mathrm{comp}}}{1 + w_{\mathrm{comp}} \cdot (p - p_0)}\right)^{-1}. \tag{5}$$

In the equation, β_{fluid} is the fluid elastic modulus that changes with temperature. w_{comp} is the compliance parameter of pipeline wall, and its value is the reciprocal of the elastic modulus β_{wall}. p_0 is the reference pressure.

The effective volume of the pipeline is

$$V_{\mathrm{eff}} = V \cdot \left[1 + w_{\mathrm{comp}} \cdot (p - p_0)\right]. \tag{6}$$

Heat exchange of the pipeline is a function of heat exchange coefficient k_{th}, pipe diameter D, pipe length l_e, and temperature difference

$$\text{dhin} = k_{\text{th}} \cdot \pi \cdot D \cdot l_e \cdot (T_{\text{ex}} - T). \tag{7}$$

For a long pipeline, considering its frequency response and fluid inertia, the flow derivative is corrected by the friction term corresponding to the frequency. The function of flow derivative is

$$\frac{\partial Q}{\partial t} = \frac{A}{\rho}\frac{\partial P}{\partial x} - g \cdot A \cdot \sin(\theta) - \frac{\text{ff} \cdot Q^2 \cdot \text{sign}(Q)}{2 \cdot D \cdot A}, \tag{8}$$

where A is the cross-sectional area, which is a function of pressure in the elastic state, θ is the inclination angle between the pipeline and the horizontal plane, and ff is the coefficient of friction.

Besides, the two-phase characteristics of the LOX cryogenic pipelines are also considered [31], which further improve the accuracy of the numerical model.

3.2. Thermal Component Model. The thermal components mainly include injectors, combustion chamber, nozzle, and cooling jacket.

The injector is mainly composed of a cavity and a nozzle, which can be regarded as a combination of a C unit (cavity) and R unit (nozzle). The corresponding parameter differences such as specific heat, viscosity, and bulk modulus in supercooled liquid, two-phase, superheated gas, and supercritical medium are considered. For a liquid nozzle, the mass flow $\dot{m}$ is

$$\dot{m} = \rho \cdot c_q \cdot \text{A} \cdot \sqrt{\frac{2 \cdot |\Delta P|}{\rho}}, \tag{9}$$

where c_q is the flow coefficient and A is the cross-sectional area of orifice. If c_q is a constant, the above equation has an infinite gradient at the origin, so the numerical model format needs to be improved as follows:

$$\begin{aligned} \lambda &= \frac{D_h}{\nu} \cdot \sqrt{\frac{2|\Delta P|}{\rho}}, \\ c_q &= c_{\text{qmax}} \cdot \tanh\left(\frac{2\lambda}{\lambda_{\text{crit}}}\right), \end{aligned} \tag{10}$$

where λ is the flow parameter, ν is the kinematic viscosity, and c_{qmax} is a constant. c_q varies approximately linearly with ΔP. The fluid Reynolds number is $\text{Re} = c_q \cdot \lambda$.

The model uses upstream parameters, so the enthalpy flow is

$$\text{dmh} = \dot{m} \cdot h\left(P_{\text{up}}, T_{\text{up}}\right). \tag{11}$$

For the gas nozzle, the mass flow is

$$\dot{m} = C_q \cdot A \cdot \Psi \cdot \sqrt{\frac{2 \cdot P_{\text{up}} \cdot \rho_{\text{up}}}{k_{\text{dp}}}}, \tag{12}$$

where k_{dp} is the pressure loss coefficient and Ψ is the flow function.

When the nozzle is not clogged, Ψ leads equation (12) to equation (9). When clogged, it is a one-dimensional compressible flow, and Ψ is related to the pressure ratio:

$$\Psi = \begin{cases} \sqrt{\dfrac{1}{1-\gamma_s}} \cdot \sqrt{\eta^{2\gamma_s} - \eta^{1+\gamma_s}} & \eta > \eta_{\text{cr}}, \\ \sqrt{\dfrac{\gamma_s}{1+\gamma_s}} \cdot \left(\dfrac{2\gamma_s}{\gamma_s + 1}\right)^{\gamma_s/1-\gamma_s} & \eta \le \eta_{\text{cr}}. \end{cases} \tag{13}$$

In the equation, γ_s is the isentropic heat factor in nonideal gas state, η is the current pressure ratio, and η_{cr} is the critical pressure ratio.

In the two-phase flow, Ψ and η_{cr} are corrected by the HEM-ω method [31]. When the flow is in a supercooled state, the model degenerates into a general incompressible fluid model.

In the combustion chamber, a zero-dimensional premixed combustion model with a fixed time delay [30] is used to simulate the low-frequency dynamic characteristics. The model is based on the assumptions of adiabatic, uniform, and ignoring liquid phase volume. The combustion model of the thrust chamber is established by the super component on AMESim platform, which realizes the fast interpolation and solution.

The mixed gas in the combustion chamber conforms to the law of mass conservation.

$$\begin{aligned} \frac{\text{dm}_c}{\text{dt}} &= \dot{m}_o(t-\tau) + \dot{m}_f(t-\tau) - \dot{m}_{\text{out}}, \\ \frac{\text{d}\rho}{\text{dt}} &= \frac{1}{V_c} \cdot \frac{\text{dm}_c}{\text{dt}}. \end{aligned} \tag{14}$$

In the equation, τ is the time delay parameter, and V_c is the volume of the combustion chamber.

According to the state equation of ideal gas, the mixing ratio in the combustion chamber is

$$\frac{\text{d}K}{\text{d}t} = (1+K)\left(\text{dm}_o - K \times \text{dm}_f\right) \cdot \frac{\text{RT}}{P_c V_c}. \tag{15}$$

In the equation, dm_o and dm_f are the mass flow of oxidant and fuel, respectively.

There are 10 main reactants and products involved in the combustion reaction, such as CO, CO_2, and H_2O. A multidimension thermodynamic database is generated by the auto CEA program, and the interpolation covers the pressure range of 0~10 MPa and the mixing ratio of 0~500. As a result, the mass fraction of each component and the

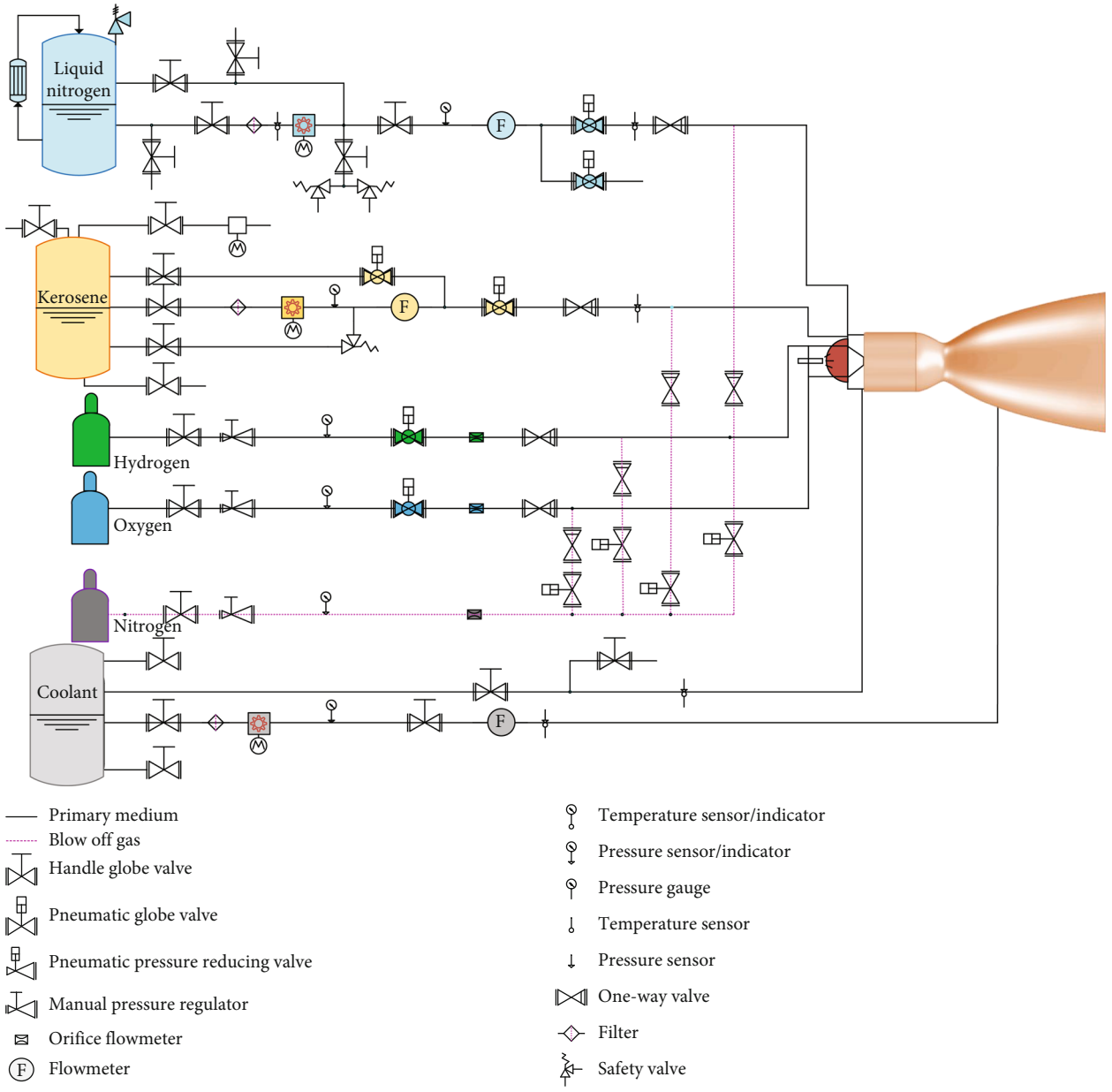

Figure 1: The structure diagram of the LRE test system.

Table 1: Main parameters of the test system.

Parameters	Flow (kg/s)	Pressure (MPa)	Accuracy
Kerosene	2.5	5	1.5%
LOX	3.5	5	1.5%
Hydrogen	0.05	5	1%
Oxygen	0.1	5	1%
Nitrogen	1.5	5	1%
Coolant	2.5	2	1%

temperature of the mixture can be quickly calculated, and the calorific value of the gas RT can be obtained:

$$\mathrm{RT} = \mathrm{RT}(K, P_c). \tag{16}$$

The dynamic equation of the combustion chamber pressure is

$$\frac{\mathrm{dP}_c}{\mathrm{dt}} = \frac{\mathrm{RT}}{V_c} \cdot \frac{\mathrm{dm}_c}{\mathrm{dt}} + \frac{P_c}{\mathrm{RT}} \cdot \frac{d(\mathrm{RT})}{\mathrm{dt}} - \frac{P_c}{V_c} \cdot \frac{\mathrm{dV}_c}{\mathrm{dt}}. \tag{17}$$

Nozzle is a key component to convert the combustion energy into mechanical energy, and it accelerates the gas flow and generates thrust. The outlet of the combustion chamber is directly connected to the nozzle, so the flow out of the combustion chamber $\dot{m}_{\mathrm{out}}$ is equal to that of the nozzle $\dot{m}_{\mathrm{nozzle}}$. Considering the real gas effect and energy loss, the calculation equation of nozzle flow under the

Table 2: Thermodynamic parameters of the thrust chamber in pretest condition.

Parameters	Combustion chamber	Throat	Exit
Temperature T (K)	2010.7	1753.2	1037.4
Characteristic velocity C^* (m/s)		1521.5	
Theoretical specific impulse I_{sp} (m/s)		2212.6	
Expansion ratio		4.55	

Table 3: Design parameters of the thrust chamber.

Parameters	Symbol	Unit	Value
Total flow	$\dot{m}$	kg/s	2.0
Mixing ratio	μ		1.3
Liquid oxygen flow	m_o	kg/s	1.13
Kerosene flow	m_f	kg/s	0.87
Chamber pressure		MPa	3
Expansion ratio	ε		5
Throat diameter	D_t	mm	36
Exit diameter	D_e	mm	80.5
Chamber diameter	D_c	mm	140
Chamber length	L_c	mm	280
Ideal thrust	F	N	4440.66

assumption of frozen flow is

$$\dot{m}_{\text{nozzle}} = A_t \cdot C_q \cdot C_m \cdot \frac{p_{\text{up}}}{\sqrt{T_{\text{up}}}}. \tag{18}$$

The upstream parameters are used in the calculation. When the loss of total pressure and total temperature is not considered, p_{up} and T_{up} are equivalent to P_c and T in the combustion chamber, respectively.

The enthalpy flow is the same as equation (11). C_m is the nozzle's flow parameter:

$$C_m = \sqrt{\frac{2\rho_{\text{up}} \cdot T_{\text{up}}}{p_{\text{up}}}}\Psi. \tag{19}$$

The engine thrust considering the environmental pressure is

$$F = \dot{m}_{\text{nozzle}} v_e + (p_e - p_a)A_e. \tag{20}$$

In the equation, v_e is the exhaust velocity.

$$v_e = \begin{cases} \sqrt{\dfrac{2}{1-\gamma_s} \cdot \dfrac{p_{\text{up}}}{\rho_{\text{up}}}} \cdot \sqrt{1 - \left(\dfrac{p_{\text{dn}}}{p_{\text{up}}}\right)^{1-\gamma_s}} & \eta > \eta_{\text{cr}}, \\ \sqrt{\dfrac{2}{1+\gamma_s} \cdot \dfrac{p_{\text{up}}}{\rho_{\text{up}}}} & \eta \le \eta_{\text{cr}}. \end{cases} \tag{21}$$

The nozzle model also considers the gas separation of the one-dimensional jet. According to the nozzle flow separation standard in reference [32], the separation position is calculated to improve the calculation accuracy of thrust.

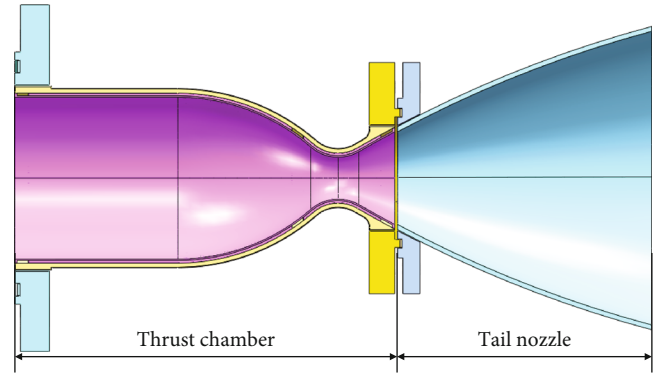

Figure 2: The structure schematic of the thrust chamber.

As for the water-cooled jacket, the Bartz method [30] is adopted to calculate the heat transfer on the gas side, and the heat exchange model of jacket flow [28] is used to calculate the heat transfer between the wall and the coolant.

3.3. Pump Model. The flow is controlled by fixed orifices, flowmeters, and pumps. There are three different pumps in the system: LOX pump, kerosene pump, and coolant pump.

The LOX pump is a BP type three-row piston pump, composed of a pump body, cylinder liners, pistons, liquid outlet valves, liquid inlet valves, some sealers, and other components. The numerical model based on AMESim platform [33] takes into account factors such as fine components, mechanical inertia, and sealing gap. The volume flow is

$$Q = -\frac{\Delta p}{12\mu l_c} r_c^3 \pi d_p \left(1 + \frac{3}{2}\left(\frac{\text{ecc}}{r_c}\right)^2\right) + \frac{v^+ + v^-}{2} r_c \pi d_p, \tag{22}$$

where Δp is the pressure difference between the front and rear of the piston, r_c is the radial clearance, d_p is the outer diameter of the piston, l_c is the contact length, μ is the average hydrodynamic viscosity, ecc is the eccentricity of the piston, and v^+ and v^- are the sleeve and piston speed, respectively.

The kerosene pump is a piston pump with an axial swash plate. Its structure is similar to other piston pumps, but there are special sealing structures such as sliding shoes and valve

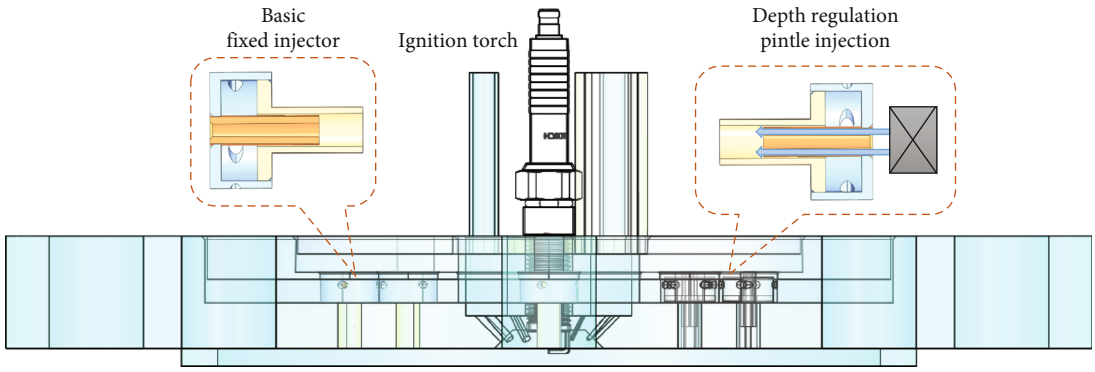

Figure 3: The head structure of the thrust chamber.

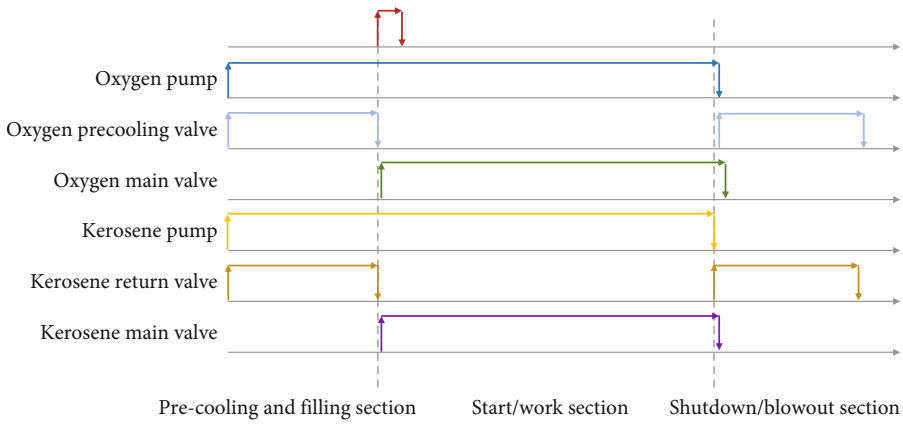

Figure 4: Working sequence of the test system.

plates. The numerical model is

$$\frac{dp_{ni}}{dt} = \frac{\beta \cdot (-Q - \sum dvol_i)}{(v_0 + \sum vol_i)} + \beta\alpha \frac{dT_{ni}}{dt},$$
$$Q = Q_{nini} + Q_{nouti} + Q_{nlspi} + Q_{nlpci} + Q_{nlbpp}, \quad (23)$$

where the vol_i is the sum of the constant volume and the variable volume of each chamber. The pressure change is determined by the total flow Q, which consists of the inlet flow Q_{nini}, the outlet flow Q_{nouti}, and the external leakage flow Q_{nlspi}, Q_{nlpci}, and Q_{nlbpp}.

The cavity of the kerosene pump is variable, and its outlet and inlet flow are calculated by the orifice flow in equation (9). The leakage model has three external leakage channels, which consists of piston-cylinder, swash plate-slipper, and sleeve-distribution plate. The average flow and efficiency are

$$Q_{Th} = \text{displ} \times \omega,$$
$$\eta_{vol} = \frac{Q_{mean}}{Q_{Th}}. \quad (24)$$

In the equation, displ is the theoretical displacement of the pump and ω is the rotation speed.

The coolant pump is a centrifugal Suter pump [8], and its parameters are corrected according to the measured rated head, flow, rotational speed, and efficiency. The power of each pump comes from a variable speed motor, which is a functional numerical model in AMESim library.

3.4. Valve Model. Almost all valve models in the system can be equivalent to variable-section orifices, which are same as equation (9) and equation (12). The safety valve adopts a self-defined logic model judged by pressure signal. The dynamic characteristics of the valve are fitted through the first-order time lag to meet the accuracy requirements.

4. Simulation and Verification

4.1. Simulation Model and Component Parameter Verification. Based on the theory of modular modeling [34], a dynamic simulation model of the LRE test system is established on the AMESim platform, and the structure is shown in Figure 5. Variable input and output interfaces are inserted into all component models, which can automatically perform variable check when the models are connected to each other. This method greatly improves the efficiency of program debugging. The main sequence and variable values of the system are controlled by piecewise functions. The whole model contains 135 state variables, corresponding to

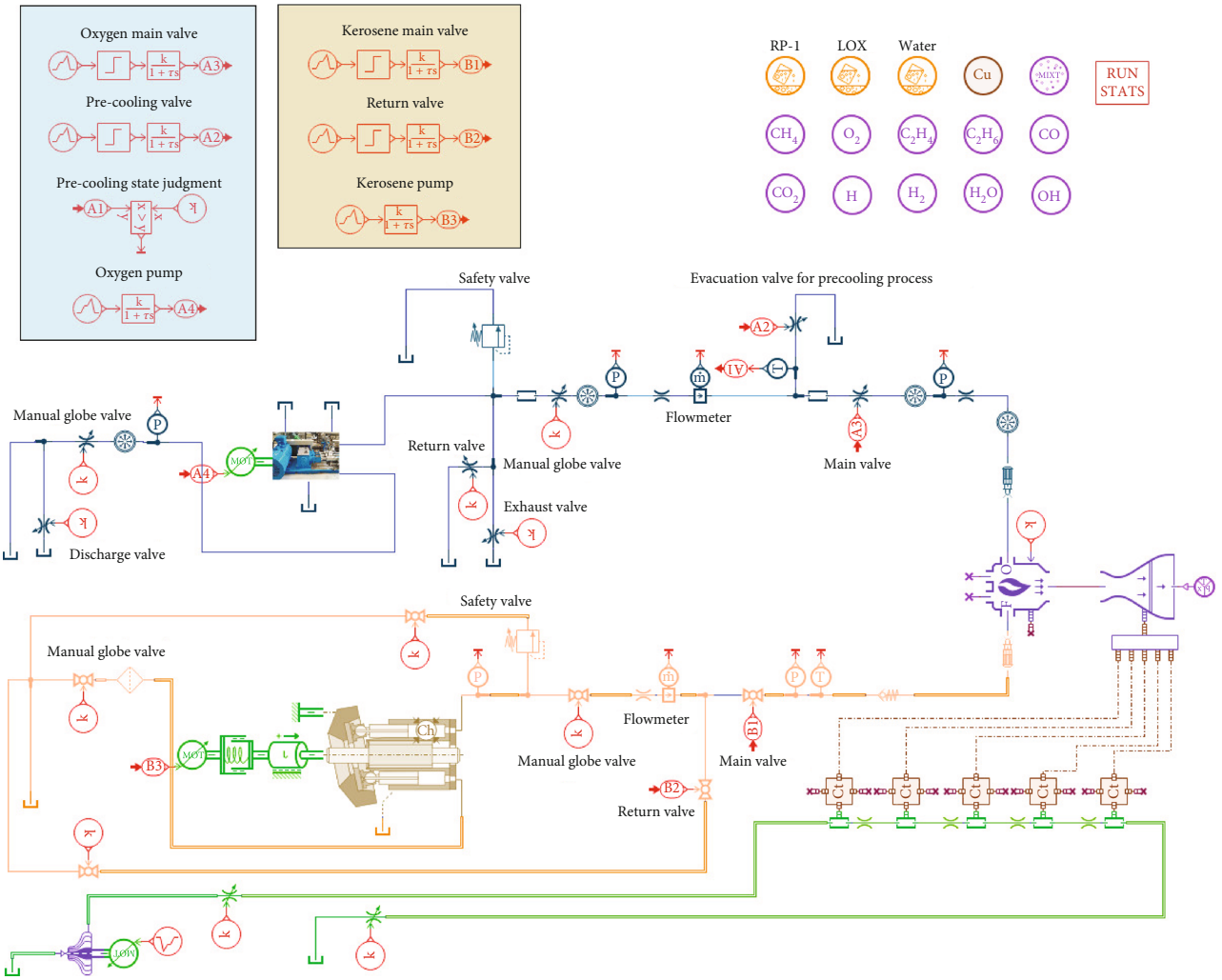

Figure 5: The structure diagram of the LRE test system.

Table 4: Parameters of the main pipelines.

Parameters	LOX	Kerosene	Coolant
Pump inlet (mm)	76.1	76.1	42.4
Pump outlet (mm)	42.4	42.4	42.4
Propellant return (mm)	50	42.4	42.4
Exhaust pipeline (mm)	25	/	/
Overflow pipeline (mm)	20	20	/

Table 5: Measured performance parameters of pumps.

Parameters	LOX	Kerosene	Coolant
Rated displacement (L)	0.25	0.125	/
Rated flow (L/min)	185	175	133.33
Rotational speed (rpm)	740	1400	2900
Rated pressure (MPa)	10	10	2
Volumetric efficiency	83.7%	82%	94%

135 dynamic equations, which can be solved by a variable step integral solver. The method avoids the dilemma of the traditional "Runge-Kutta" method in discontinuities of system equations.

The main pipeline parameters are shown in Table 4, where the elastic modulus of the pipeline wall is considered in the numerical model. Subtracting the wall thickness, the inner diameter of the main propellant inlet pipeline is 65.9 mm, and the inner diameter of the outlet pipeline is 32.4 mm.

The pump models mainly include three-row piston pump, swash plate axial piston pump, and centrifugal pump. The main structure and performance parameters are shown in Table 5, most of which are obtained from actual tests.

As shown in Figure 6 and Table 6, the three-row piston pump model consists of three main submodels: the rotation and translational mechanical model, the piston model, and the switch valve model. These parameters about cylinder, shaft inertia, dead zone, and key leakage gaps are considered. The contact length of the piston and cylinder is 67 mm and the piston stroke is 62 mm. The volumetric efficiency of the pump drops to about 87.6% under the simulated condition of 740 rpm and 10 MPa backpressure, which is slightly higher than the actual measurement. The model error is

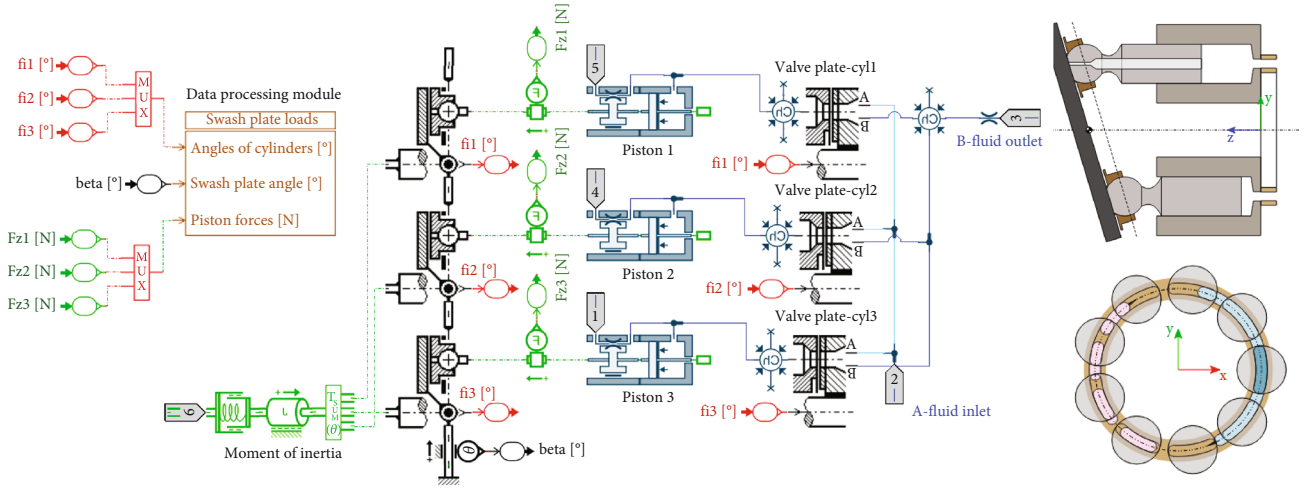

Figure 6: The LOX three-row piston pump model (left) and kerosene piston pump (right).

Table 6: Partial model parameters for pump simulation.

Parameters	LOX	Kerosene
Piston diameter (mm)	40	26
Number of pistons	3	9
Piston clearance (mm)	0.065	0.035
Piston eccentricity	0	0

about 4% related to the actual piston eccentricity and other structural parameters.

The main input parameters of the kerosene piston pump model are swash plate angle (16.7°), valve plate clearance (0.02 mm), piston/barrel clearance (0.035 mm), and slipper clearance (0.0175 mm). As shown in Figure 6, the model considers parameters such as unloading grooves and swash plate structures. The real flow test at 1400 rpm shows that the model error is less than 2.1%, and more results are shown in Figure 7.

To ensure the simulation accuracy, the geometric dimensions of other components are consistent with the actual parameters, and the valve flow coefficient and other data are calibrated according to the rated parameters in the manufacturing process. The elastic modulus of the pipeline wall and the thermal conductivity of the material are referred to the AMESim material library and the chemical kinetics database (National Institute of Standards and Technology, NIST).

4.2. Preliminary Verification of Results. The model accuracy is checked by the components cold test and the design parameters, and the dynamic model of the test system is solved. The main parameters such as thrust, flow, combustion chamber temperature, pressure, mixing ratio, and heat transfer under the pretest are shown in Figures 8–10.

Figure 8 shows that in the stable section (the stable speeds of the kerosene and LOX pumps are 590 and 271 rpm, respectively), the average total flow is 1.96 kg/s, and the fluctuation range is about 1.5%, which is basically consistent with the target value. The average thrust at sea

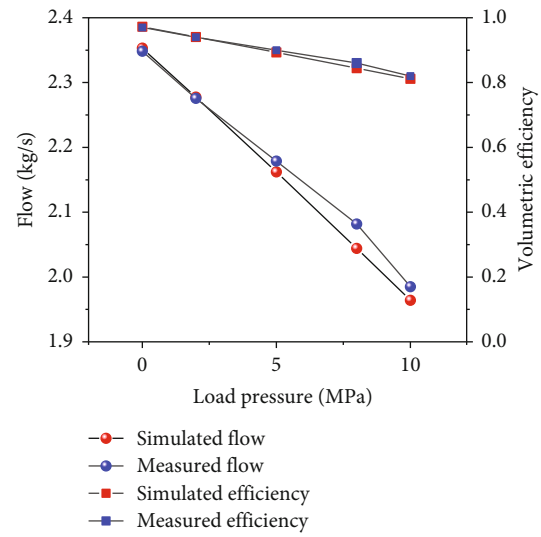

Figure 7: The verification of kerosene piston pump model.

level is 4024 N (90.62% of that in perfect theoretical combustion and expansion flow), and the fluctuation range is about 5%. The results prove that the thrust fluctuation is mainly caused by the pump pressure pulsation, pipeline elasticity, propellant inertia, and compressibility. Compared with the pump outlet, the pulsation of the thrust chamber is attenuated to a certain extent, which is beneficial to the working condition of the test system.

Figure 9 depicts that the average temperature is 1973 K (temperature statistics with 1 s as the sliding window) and the absolute pressure is about 2.9 MPa in the combustion chamber. The fluctuation range of pressure is 2.83~2.98 MPa, and the main frequency is 13.65 Hz. The error of the pressure extreme value compared with the system scheme is 5.67%, and the average error is less than 3.3%. The mixing ratio in the stable section is about 1.3, which is in line with the expectation. There exist slight temperature and pressure fluctuations in Figure 9, which is due

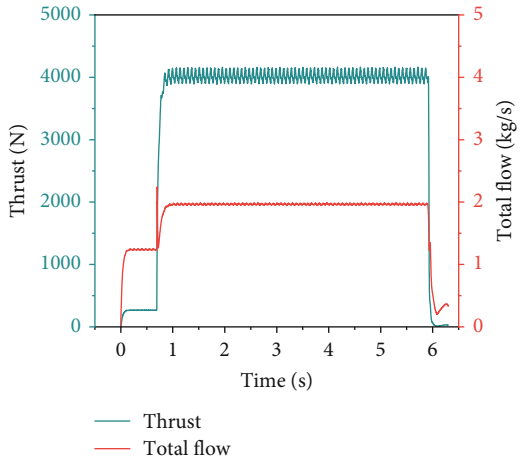

Figure 8: The thrust and total flow of the pretest condition.

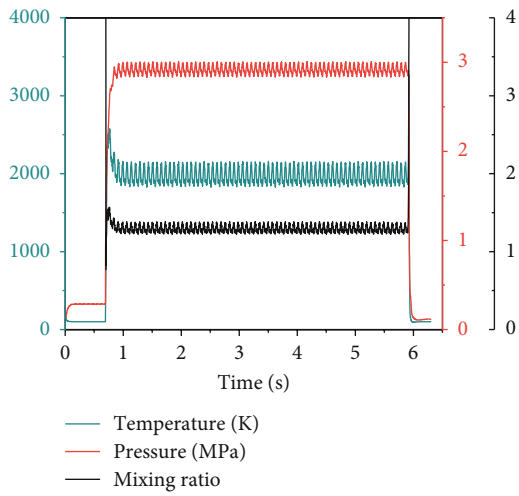

Figure 9: Thermal conditions of the combustion chamber.

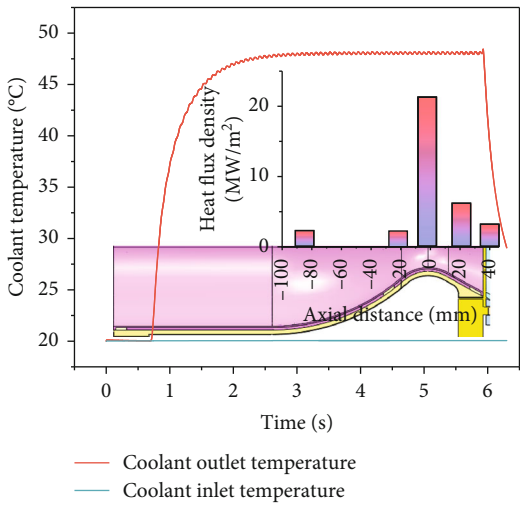

Figure 10: The diagram of the thrust chamber cooling and the nozzle heat exchange.

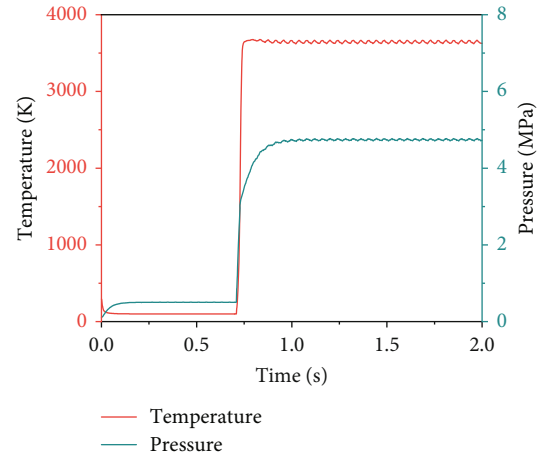

Figure 11: The start-up process in variable thrust conditions.

to the positive displacement pumps of LOX and kerosene have inherent pressure and flow pulsation in the process of operation. Meanwhile, there are damping and volume effects of complex pipelines and nozzles. The combined effect causes the fluctuation in the flow of each propellant, which directly leads to the oscillation of the mixing ratio in the combustion chamber. When the mixing ratio is between 1 and 3, the mixing ratio is the main reason for the change of temperature. In other word, the pump speed as an input parameter determines the LOX and kerosene flow, which in turn changes the mixing ratio and total flow, and ultimately determines the variation in temperature and pressure of the combustion chamber.

The cooling and heat exchange of the thrust chamber are shown in Figure 10. The simulated flow of the coolant is about 2.03 kg/s, and the average temperature rise is about 28°C, which meets the design requirements. The heat flux density of the thrust chamber throat is the largest, about 21 MW/m^2. Meanwhile, the specific impulse is about 208 s under the pretest condition.

5. Results and Discussion

Based on the system model in pretest condition, the control variables such as time sequence and parameters are adjusted to obtain characteristics of the engine test system under start-up, shutdown, and variable thrust conditions. The pressure of the combustion chamber as the main control variable includes four stages: 5 MPa, 3 MPa, 2 MPa, and 1 MPa, and the mixing ratio in steady state is set to 2.67. During the actual test process, the control system can slightly adjust the pump speed and the flow area of valves according to the combustion chamber pressure and mixing ratio to achieve precise control of thrust.

5.1. Start-Up Process. The start-up process under variable thrust conditions is shown in Figure 11. The oxygen main valve is opened and the ignition torch is ignited at 0 s. After the propellant filling process (about 0.7 s), the thrust chamber reaches the rated temperature and pressure, and the transition process of ignition delay is about 200 ms.

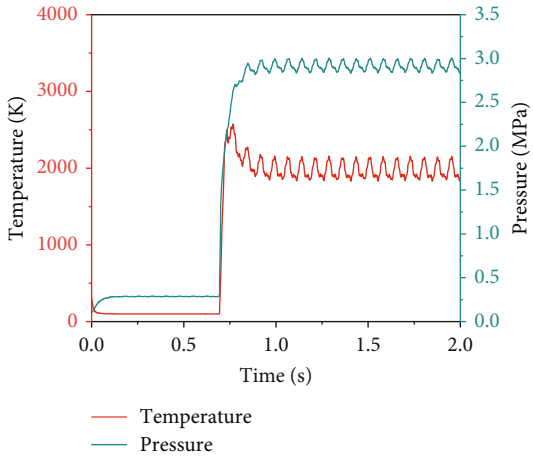

Figure 12: The start-up process of the pretest condition.

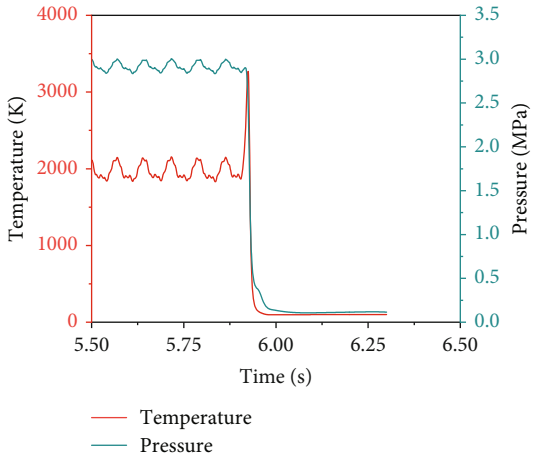

Figure 13: Shutdown process in pretest condition.

The first stage pressure (4.8 MPa) and theoretical temperature (3654 K) are relatively high, but the impact of starting shock is small thanks to the resistance of the pipelines under high flow conditions. On the other hand, the mixing ratio in the pretest condition is 1.3 and the stable temperature is about 2000 K. The early injection of liquid oxygen leads to the increase of the actual mixing ratio and the short temperature shock (Figure 12). The rated value is restored after about 190 ms, indicating a smooth start-up process. In addition, it is observed that the temperature and pressure of the combustion chamber oscillated slightly, which is due to the large effect of the gas temperature on the mixing ratio near the oil-rich combustion operating point (temperature is highly sensitive to low mixing ratio). The positive displacement pumps have inherent periodic pulsations, which will directly lead to significant fluctuations in the mixing ratio, and thus promote the changes in the combustion chamber temperature and pressure under the pretest condition. Meanwhile, for the combustion chamber and nozzle with fixed sizes, the changes in temperature and total flow lead to similar periodic changes in pressure. The phenomenon can also be seen in Figure 13.

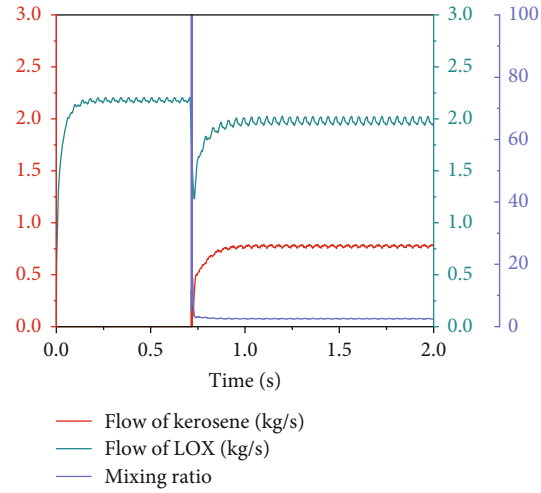

Figure 14: Propellant flow at the moment of start-up process in variable thrust conditions.

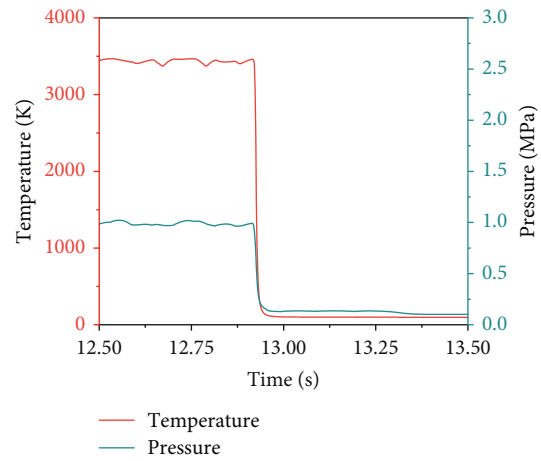

Figure 15: Shutdown process in variable thrust condition.

Figure 14 shows the start-up transient process of LOX and kerosene flow under pretest condition. During the pressure generation in the thrust chamber, there is a brief jump in the LOX injection flow, which is caused by the pressure jump triggered by the instantaneous ignition. The magnitude of the pressure fluctuation depends on the leakage of the propellant pumps, the elasticity of pipelines, and the compressibility of the propellant. Due to the inherent flow characteristics of the positive displacement pumps, the stable operation of the electric pump allows the propellant flow to reach the rated value around 240 ms after ignition.

5.2. Shutdown Process. Figures 13 and 15 show the shutdown process of the pretest and variable thrust test conditions. The transition time is about 80~100 ms, and the impulse fluctuation is very small. The main reason is that the thrust chamber is cooled by water and the shutdown valve is close to the head of the thrust chamber, which effectively avoids the residue of unburned propellant.

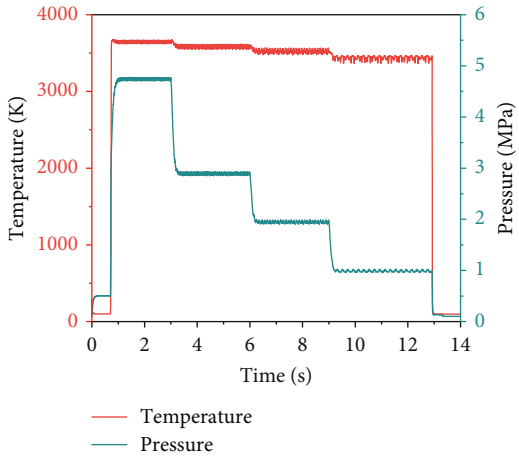

Figure 16: Temperature and pressure changes of the combustion chamber in variable thrust condition.

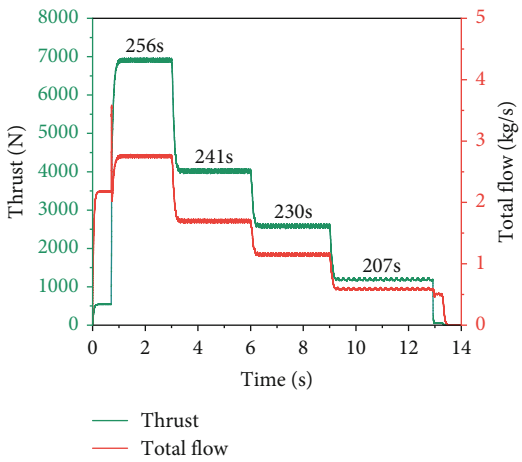

Figure 17: Thrust/specific impulse and total flow change in the process of variable thrust.

It is worth noting that the LOX main valve closing is delayed by about 50 ms compared to the kerosene circuit, which causes the temperature of the thrust chamber briefly climb at the moment of shutdown in the pretest condition (<3200 K).

5.3. Variable Thrust Process. The variable thrust test process is carried out under operating conditions close to the optimum mixing ratio. Figure 16 shows that the temperature of the thrust chamber decreases slightly during the whole process, and the pressure of each stage is about 4.8 MPa, 2.9 MPa, 1.9 MPa, and 1.0 MPa, respectively. The results confirm that the flow control is relatively synchronous, the state transition is smooth, and the adjustment response time is about 300 ms.

Figure 17 shows that the variable range of the thrust is about 5 : 1. In the test process, taking the high working condition of 6900 N (specific impulse 256 s) as the standard point, the thrust of each stage drops to 4000 N (58%), 2600 N (37.6%), and 1200 N (17.4%, specific impulse 207 s), respectively.

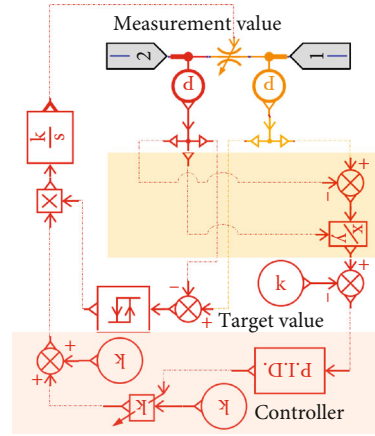

Figure 18: The PID control structure and function simulation model of the pintle injector.

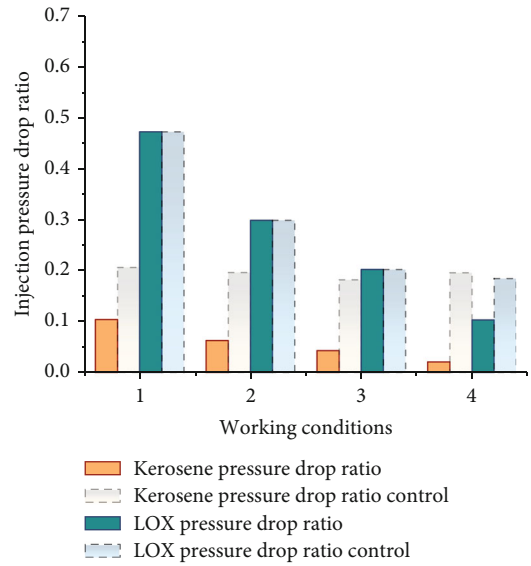

Figure 19: Injection pressure drop ratio of the thrust chamber.

The change process of thrust, specific impulse, and total flow of the engine is shown in Figure 17. The thrust is synchronized with the flow regulation transition process. Under the minimum thrust condition, the propellant pump is at 12.2% (LOX) and 7% (kerosene) of full flow output, respectively. The total flow is gradually reduced from 2.7 kg/s to 0.6 kg/s. The corresponding LOX flow is reduced from 1.97 kg/s (492 rpm of pump speed) to 0.43 kg/s (99 rpm of pump speed), and the kerosene flow is reduced from 0.73 kg/s (578 rpm of pump speed) to 0.17 kg/s (118 rpm of pump speed).

Considering the risk that the pressure drop of the injector is too low to ensure normal combustion under low working conditions, a special injector is designed for the depth variable thrust working conditions. The pintle injector is driven by a stepper motor, and its PID control structure and function simulation model are shown in Figure 18. The model parameters are derived from modular testing of the system inertia. Based on the injector model, the oxidant

and fuel injection areas can be automatically adjusted according to the combustion chamber pressure and the ratio of injection pressure drop.

Figure 19 compares the average pressure drop ratio at each stage before and after the use of the pintle injector in the 5 : 1 variable thrust process. Without taking control, the pressure drop ratio decreases significantly as the engine working condition decreases. The pressure drop ratio of the LOX injection with fixed injectors rapidly decreases from 45% to 12%, while the kerosene injector also gradually decreases, and even the pressure drop ratio of the third and fourth stages is less than 5%, which may lead to unstable phenomenon such as surge during the combustion process. On the contrary, the histogram of the dotted line in Figure 19 shows that better pressure drop ratio control can be achieved by pintle injectors with adjustable cross section areas. Compared with the fixed injector, the pressure drop ratio of the kerosene pintle injector always remains stable at about 20%, which can well avoid the risk of unstable combustion in the combustion chamber. Moreover, the pressure drop ratio of the LOX pintle injector gradually decreases as the reduction of working conditions and eventually also stabilizes around 20%.

The target value of the pressure drop ratio (20% in the test) is set by the PID controller, as shown in Figure 18, which means the pintle injector with PID controller is useful to adjust and stabilize the injection pressure drop ratio in the depth variable thrust LRE, thus avoiding the adverse effects of the pressure drop ratio on the engine. Therefore, the model is of great value for the regulation and control of deep variable thrust engines in the future.

6. Conclusions

A LOX/kerosene rocket engine system driven by electric positive displacement pumps is presented in the manuscript, which is an important branch in the field of reusable variable thrust LRE. The multidisciplinary modular dynamic simulation method based on AMESim platform is used to analyze the unique LOX/kerosene engine system. The method comprehensively considers the characteristics of complex components in the engine and realizes the fast module assembly and variable step size solution. The main conclusions on the scheme verification and dynamic characteristics analysis are as follows:

(1) The LOX/kerosene rocket engine test system is stable for ignition, stage turning, and shutdown process, with a specific impulse of 256 s and a continuously variable thrust capability of 5 : 1, thus confirming the feasibility of the overall design

(2) The modular system simulation method has strong expansibility, so the dynamic characteristics of related engine systems can be analyzed quickly. The error of the simulation model about LOX three-row piston pump and kerosene swash plate piston pump is less than 5% compared with the measured results, which confirms the high precision of the model. Besides, the model is more detailed considering the complex flow, heat exchange, and combustion problems

(3) The safety margin of the test system meets the actual usage requirements. By controlling the cumulative amount of LOX and kerosene propellant, the short-term (190 ms) adverse effect of LOX accumulation on the temperature of the thrust chamber can be effectively avoided

(4) The variable thrust process can be changed by adjusting the propellant supply, and the electric pumps have a prominent advantage in the adjustment of test conditions. The use of pintle injector based on PID control is helpful to further improve the deep variable thrust test capability of the system

Data Availability

The data used to support the findings of this study are available from the corresponding authors upon request.

Conflicts of Interest

The authors declare that they have no conflicts of interests.

Acknowledgments

This work is supported by the Fundamental Research Project (No. 20195208003).

References

[1] G. P. Sutton, "History of liquid propellant rocket engines in the United States," *Journal of Propulsion and Power*, vol. 19, no. 6, pp. 978–1007, 2003.

[2] Y. Jin, X. Xu, Q. Yang, and S. Zhu, "Numerical investigation of flame appearance and heat flux and in a deep- throttling variable thrust rocket engine," *Aerospace Science and Technology*, vol. 88, pp. 457–467, 2019.

[3] V. Rachuk, N. Goncharov, Y. Martinyenko, and T. Fanciullo, "Evolution of the RD-0120 for future launch systems," in *32nd Joint Propulsion Conference and Exhibit*, Lake Buena Vista, FL, U.S.A, 1996.

[4] E. Seedhouse, *SpaceX: Making Commercial Spaceflight a Reality*, Springer Science & Business Media, 2013.

[5] X. Guo, "Liquid rocket engine test," Aerospace Press, 1990.

[6] Y. Zhang, K. Liu, and M. Cheng, "Dynamics theory and application of liquid rocket motor," Science Press, 2005.

[7] H. H. Xu, "Research on start-up process of liquid oxygen kerosene supplementary combustion engine," *The Eleventh Research Institute of the Sixth Research Institute of China Aerospace Science and Technology Corporation*, 2003.

[8] T. Y. Cao, "Rocket engine dynamics," *National University of Defense Technology Press*, 2004.

[9] M. Powell, P. Butler, and L. Beck, "Ground test simulation of rocket engine start transients," in *11th Propulsion Conference*, Anaheim, CA, U.S.A, 1975.

[10] C. M. Meyer and W. A. Maul, "The application of neural networks to the SSME startup transient," in *Presented at the 27th Joint Propulsion Conference*, Sacramento, CA, U.S.A, 1991.

[11] A. Kanmuri, T. Kanda, Y. Wakamatsu, Y. Torii, and E. Kagawa, "Transient analysis of LOX/LH2 rocket engine (LE-7)," in *25th Joint Propulsion Conference*, Monterey, CA, U.S.A, 1989.

[12] W. Zhang, Q. Tian, and Z. G. Xu, *Failure Characteristics Analysis and Diagnosis of Liquid Missile Engine*, National Defense Industry Press, 2014.

[13] Y. Q. Li, H. J. Liu, H. H. Xu, and H. Y. Chen, "Research progress of liquid rocket engine dynamic characteristics," *Rocket Propulsion*, vol. 43, no. 5, p. 6, 2017.

[14] C. Goertz, "A modular method for the analysis of liquid rocket engine cycles," in *AIAA Joint Propulsion Conference & Exhibit*, San Diego, CA, U.S.A, 1995.

[15] M. Binder, "An RL10A-3-3A rocket engine model using the rocket engine transient simulator (ROCETS) software," in *Joint Propulsion Conference and Exhibit*, Monterey, CA, U.S.A, 1993.

[16] V. Leudiere, G. Albano, G. Ordonneau, J. Masse, and B. Legrand, "CARINS: a versatile and flexible tool for engine transient prediction development status," in *24th International Symposium on Space Technology and Science*, Tokyo, Japan, 2004.

[17] N. Yamanishi, T. Kimura, M. Takahashi, K. Okita, M. Atsumi, and H. Negishi, "Transient analysis of the LE-7A rocket engine the rocket engine dynamic simulator (REDS)," in *40th AIAA/ASME/SAE/ASEE Joint Propulsion Conference and Exhibit*, Fort Lauderdale, Florida, 2004.

[18] A. Isselhorst, "HM7B simulation with ESPSS tool on ARIANE 5 ESC-A upper stage," in *AIAA/ASME/SAE/ASEE Joint Propulsion Conference and Exhibit*, Nashville, TN, 2010.

[19] H. Pan and L. H. Zhang, "Application of AMESim software in dynamic simulation of liquid rocket engine system," *Rocket Propulsion*, vol. 37, no. 3, pp. 6–11, 2011.

[20] Z. Z. Fan, M. C. Huang, Y. Yu, and H. W. Zhu, "Modular modeling of the working process of space propulsion system," *Journal of National University of Defense Technology*, vol. 29, no. 2, pp. 29–33, 2007.

[21] L. H. Zhang, W. Li, and N. Duan, "Modular general simulation of liquid rocket motor," *Journal of Aerospace Power*, vol. 26, no. 3, pp. 687–691, 2011.

[22] C. M. Wang, X. G. Zhang, Y. S. Gao, and H. Chen, "Research on the acceleration spin-up scheme of oxygen pre-pressure pump during the starting process of liquid oxygen kerosene supplemented combustion engine," *Propulsion Technology*, vol. 41, no. 7, p. 8, 2020.

[23] H. Y. Chen, H. J. Liu, and J. H. Chen, "Forced start process of supplementary combustion cycle engine," *Journal of Aerospace Power*, vol. 30, no. 12, pp. 3010–3016, 2015.

[24] J. J. Li, "A fast method for dynamic simulation of low temperature engine system," *Missile and Space Launch Technology*, vol. 1, no. 5, pp. 13–17, 2012.

[25] D. Y. Zheng, H. Y. Wang, and J. Hu, "Research on transient characteristics of high-thrust hydrogen-oxygen engine," *Propulsion Technology*, vol. 42, no. 8, p. 9, 2021.

[26] W. Zhang, D. W. Sun, W. H. Chen, R. Gao, J. Y. Chen, and J. L. Xie, "Simulation of water hammer in liquid nitrogen supplying system based on AMESim," *Journal of Aerospace Power*, vol. 37, no. 2, pp. 366–374, 2022.

[27] Y. Liu, B. S. Fu, J. G. Yang, G. He, Y. He, and P. Liu, "Modeling and simulation of electric pump-pressure liquid rocket engine system," *Manned Aerospace*, vol. 25, no. 1, p. 9, 2019.

[28] P. Cui, J. Song, Q. L. Li, L. W. Chen, T. Liang, and J. Sun, "Dynamics modeling and simulation analysis of electric pump-pressure liquid kerosene variable thrust rocket engine: part I-single-point condition analysis," *Chinese Journal of Aeronautics and Astronautics*, vol. 43, no. 1, p. 15, 2022.

[29] Glickman, "Automatic adjustment of liquid rocket motor translated by Gu Mingchu," *Aerospace Press*, 1995.

[30] Y. F. Zhai, "Research on dynamic simulation of expansion cycle engine thrust regulation process," *China Aerospace Science and Technology Corporation*, 2017.

[31] Siemens, *Simcenter AMESim 2020.1 Two Phase Flow Library User's Guide*, Siemens Industry Software NV, 2020.

[32] R. Stark, "Flow separation in rocket nozzles, a simple criteria," in *41th Joint Propulsion Conference & Exhibit*, Tucson, Arizona, 2005.

[33] Siemens, *Simcenter AMESim 2020.1 Thermal Hydraulic Component Design Library User's Guide*, Siemens Industry Software NV, 2020.

[34] Q. Su, J. Wang, M. Yan, Z. Sun, B. Zha, and W. Huang, "The dynamic model of the high-thrust orbital maneuvering engine with storable propellant," *Journal of Physics: Conference Series*, vol. 2364, no. 1, article 012014, 2022.